Mod Pathol 38 (2025) 100771

MODERN PATHOLOGY

USCAP UNITED STATES AND CANADIAN ACADEMY OF PATHOLOGY
Advancing Pathology Together

Journal homepage: https://modernpathology.org/

Research Article

Artificial Intelligence–Based Single-Cell Analysis as a Next-Generation Histologic Grading Approach in Colorectal Cancer: Prognostic Role and Tumor Biology Assessment

Vincenzo Mitchell Barroso[a,b], Zhilong Weng[b], Lennert Glamann[c], Marcus Bauer[c], Claudia Wickenhauser[c], Thomas Zander[d], Reinhard Büttner[b], Alexander Quaas[b], Yuri Tolkach[b,*]

[a] *Medical Faculty, University of Cologne, Cologne, Germany;* [b] *Insitute of Pathology, University Hospital Cologne, Cologne, Germany;* [c] *Institute of Pathology, University Hospital Halle, Martin Luther University Halle-Wittenberg, Halle (Salle), Germany;* [d] *Clinic of Internal Medicine, Oncology, University Hospital Cologne, Cologne, Germany*

ARTICLE INFO

Article history:
Received 6 November 2024
Revised 16 March 2025
Accepted 1 April 2025
Available online 11 April 2025

Keywords:
artificial intelligence
colorectal cancer
grading
hematoxylin and eosin
prognosis
single-cell

ABSTRACT

The management of colorectal carcinoma (CRC) relies on pathological interpretation. Digital pathology approaches allow for development of new potent artificial intelligence–based prognostic parameters. The study aimed to develop an artificial intelligence–based image analysis platform allowing fully automatized, quantitative, and explainable tumor microenvironment analysis and extraction of prognostic information from hematoxylin and eosin–stained whole-slide images of CRC patients. Three well–characterized, multi-institutional patient cohorts were included (patient n = 1438, whole-slide image n > 2400). The developed image analysis platform implements quality control and established algorithms to segment tissue and detect cell types. It enabled systematic analysis of immune infiltrate, assessing its prognostic relevance, intratumoral heterogeneity, and biological concepts across multiple survival end points. Analyzing single-cell types and their combinations reveals independent, prognostic parameters, highlighting significant intratumoral heterogeneity, especially in the biopsy setting, which must be accounted for. A key morphologic concept related to tumor control by the immune system is described, resulting in a capable, independent prognostic parameter (tumor "out of control"). Our findings have direct clinical implications and can be used as a foundation for updating the existing CRC grading systems.

Introduction

Colorectal cancer (CRC) is one of the most common and most aggressive malignant epithelial tumors.[1] There is constant demand for new diagnostic, prognostic, and predictive biomarkers that can allow personalization of therapy approaches. Common pathological variables, such as pT stage, pN stage, histologic grade, microsatellite instability (MSI), are still main sources of prognostic information that determine all relevant clinical decisions.[2] One research group based on comprehensive investigation of microenvironment in CRC using gene expression profiling and immunohistochemistry developed ImmunoScore parameter with significant prognostic risk stratification capabilities.[3,4] This parameter, however, requires additional immunohistochemistry stains and rather complex bioinformatical analysis and finds limited usage in clinical routine.

* Corresponding author.
E-mail address: yuri.tolkach@gmail.com (Y. Tolkach).

https://doi.org/10.1016/j.modpat.2025.100771

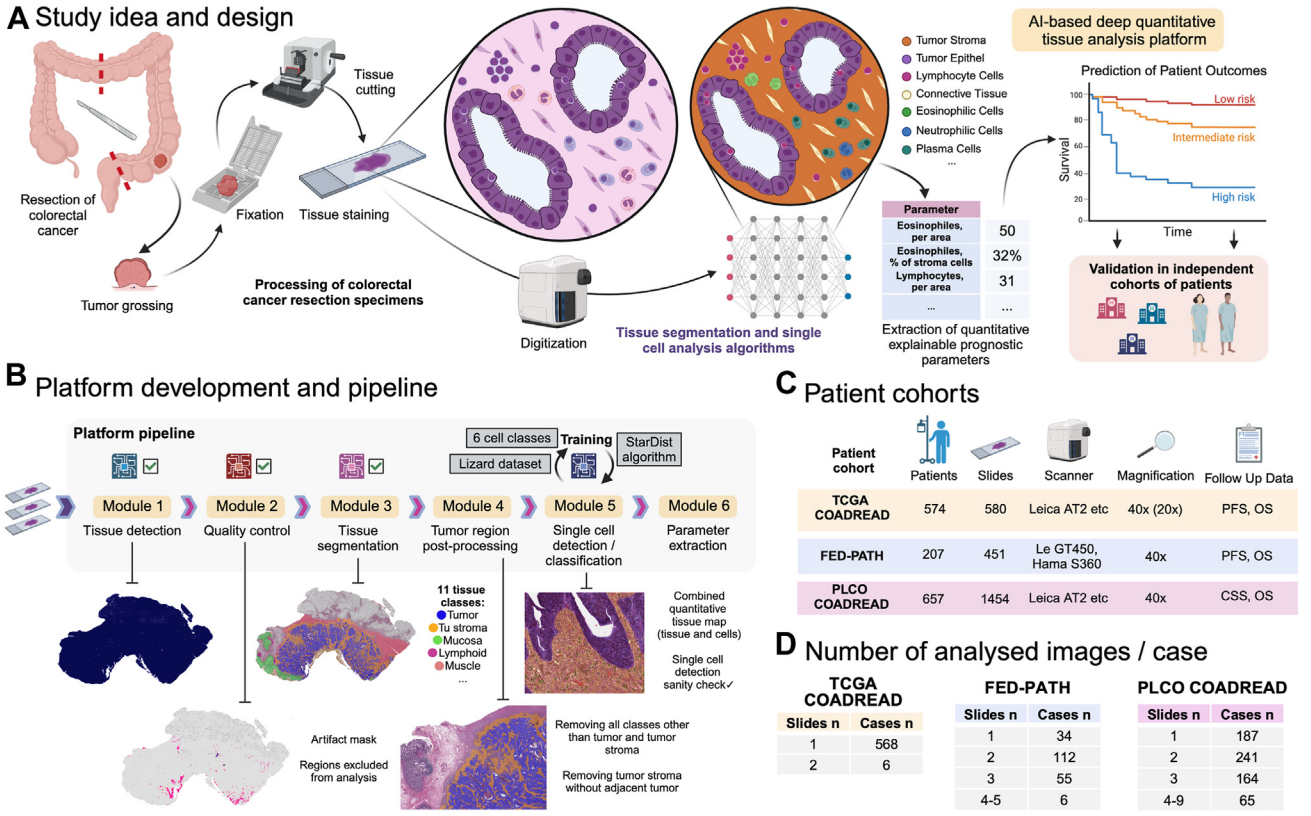

Figure 1.
Principle of artificial intelligence–based image analysis platform for colorectal cancer specimens and study cohorts. (A) Routine pathological evaluation of colorectal specimens consists of tissue fixation, embedding, and cutting, resulting in histologic sections that are stained with hematoxylin and eosin. These sections, when digitized, can be a valuable source of prognostic information, especially when single-cell populations in tumor microenvironment are analyzed. The aim of this study was to create an image analysis platform that enables fully quantitative and explainable analysis of different cell populations in tumor microenvironments. This analysis results in the development of prognostic parameters for survival prediction in CRC patients. (B) The principle of the developed platform. Modules 1 to 3 were trained and validated in previous studies and reused in the platform in an integrative manner. Module 5 was trained using state-of-the-art data set/algorithm for cell detection and classification. Module 6 analyzes raw information from the pipeline, extracts, and quantifies single cell–based parameters. (C) Three multi-institutional patient cohorts were used for this study. The TCGA cohort was primarily used for exploration and FED-PATH and PLCO cohorts for independent validation of prognostic parameters. (D) In the TCGA cohort only one slide with tumor was available for each patient, whereas multiple slides with tumor tissue were available for analysis in the 2 other cohorts. Detailed information on the number of analyzed whole-slide images per patient case is provided. OS, overall survival; PFS, progression-free survival; PLCO, Prostate, Lung, Colorectal, and Ovarian Cancer Screening Trial; TCGA, The Cancer Genome Atlas.

Computational pathology and artificial intelligence (AI)–based image analysis of histologic sections emerges as an important source of a new generation of diagnostic, prognostic, and predictive biomarkers for malignant tumors.[5,6] Several studies have addressed the prognosis in patients with CRC through automated analysis of routine hematoxylin and eosin (H&E)–stained whole-slide images digitized at high resolution (×400).[7-23] These involve, for example, analysis of tumor tissue composition, intratumoral lymphocytes, tumor budding, and tumor-to-stroma ratio. Some studies showed that useful features relevant for prognosis could be extracted automatically without defining any of them manually.[7,8,11,14] Only one study explored immune and stromal cells beyond intratumoral lymphocytes, using traditional algorithms.[23] Understanding the impact of different cell types in the tumor environment could improve prognostic accuracy and reveal insights into tumor biology with clinical implications.

In this study, we developed image analysis platform (Fig. 1A, B) for H&E-stained colorectal tumor samples. The platform allows full quantitative deciphering of the tumor microenvironment resulting in a number of clinically relevant, explainable prognostic parameters and new prognostic systems.

Materials and Methods

Patient Cohorts

Three multi-institutional patient cohorts of patients with resectable CRC were included (Fig. 1C, Table). Two well-characterized cohorts are from large trials: The Cancer Genome Atlas (TCGA) CRC cohort and Prostate, Lung, Colorectal, and Ovarian Cancer Screening Trial (PLCO) CRC cohort. One further cohort (FED-PATH) is from 2 tertiary referral centers (University Hospital Cologne/UKK and University Hospital Halle, Germany; years 2012-2021). All patients included were neoadjuvant-therapy naïve (eligibility criterion). The details on slide digitization are provided in Figure 1C, D. One additional biopsy cohort was used for validation of new parameters. This included routine diagnostic cases (primary diagnosis of CRC and endoscopic biopsies; n = 61) from a pathology institute (UKK) from years 2019 to 2020 (consecutive cases) gathered in course of the previous study.[24] Nine of 61 cases were of the status MSI, whereas in 5 patients, MSI status was unknown.

Table
Clinicopathological characteristics of the study cohorts

Parameter	I. TCGA cohort (n = 574)		II. FED-PATH cohort (n = 207)		III. PLCO cohort (n = 657)	
	n	%	N	%	n	%
Sex						
Female	272	47.4	78	37.7	277	42.2
Male	302	52.6	129	62.3	380	57.8
pT stage						
pT1	17	3.0	11	5.3	85	12.9
pT2	101	17.6	37	17.9	149	22.7
pT3	389	67.8	118	57.0	373	56.8
pT4	64	64	39	18.8	40	6.1
Unknown	3	0.5	2	1.0	10	1.5
pN stage						
pN0	323	56.3	122	58.9	382	58.2
pN1	142	24.7	40	19.3	165	25.1
pN2	108	18.8	42	20.3	87	13.2
Unknown	1	0.2	3	1.4	23	3.5
UICC stage						
I	99	17.2	30	14.5	183	27.9
II	205	35.7	47	22.7	164	25.0
III	169	29.4	17	8.2	180	27.3
IV	81	14.1	52	25.1	59	9.0
Unknown	20	3.5	61	29.5	71	10.8
L status						
L0	313	54.5	n/a	-	n/a	-
L1	219	38.2	n/a	-	n/a	-
Unknown	42	7.3	n/a	-	n/a	-
V status						
V0	383	66.7	127	61.4%	n/a	-
V1	128	22.3	68	32.9%	n/a	-
Unknown	63	11.0	12	5.8%	n/a	-
Pn status						
Pn0	168	29.3	n/a	-	n/a	-
Pn1	58	10.1	n/a	-	n/a	-
Unknown	348	60.6	n/a	-	n/a	-
MSI status						
MSS	397	69.2	108	52.2%	n/a	-
MSI-H	94	16.4	14	6.8%	n/a	-
MSI-L	80	13.9	-	-	n/a	-
Unknown	3	0.5	85	41.1%		
Localization						
Colon	425	74.0	163	78.7%	569	86.6
Rectum	149	26.0	44	21.3%	88	13.4
PFS						
Progression	114	19.9	91	44.0%	n/a	-
Censored	355	61.8	116	56.0%	n/a	-
Not available	105	18.3	-	-	n/a	-
OS						
Alive	437	76.1	133	64.3	284	43.2
Deceased	116	20.2	67	32.4	373	56.8
Not available	21	3.7	7	3.4	-	-
CSS						
Alive	n/a	-	n/a	-	507	77.2
Deceased	n/a	-	n/a	-	150	22.8
Not available	n/a	-	n/a	-	-	-
Follow-up duration						
Mean (SD), mo	29.3 (24.6)		36.4 (29.8)		134.9 (7.9)	
Range, mo	1-151		1-124		1-293	
Age, y						
Min	31		28		55	
Max	90		92		87	
Mean	66.1		65.9		69.3	
Median	67		67		70	

CSS, cancer-specific survival; L, lymphovascular invasion; MMRd, mismatch repair deficiency; MSI, microsatellite instability; MSS, microsatellite stability; OS, overall survival; PFS, progression-free survival; PLCO, Prostate, Lung, Colorectal, and Ovarian Cancer Screening Trial; pMMR, proficient mismatch repair; Pn, perineural invasion; SD, standard deviation; TCGA, The Cancer Genome Atlas; V, vascular invasion; UICC, The Union for International Cancer Control.

Single-Cell Detection and Classification Algorithm: Training

A StarDist algorithm[25] (winning solution in CONIC challenge[26]) was used to train the model using a Lizard data set[27] (details in Supplementary Methods section) allowing detection of epithelial cells, lymphocytes, plasma cells, neutrophils, eosinophils, and connective tissue cells.

Integral Tissue Analysis Platform

The computational platform established for this study includes 4 deep learning algorithms and several postprocessing and parameter extraction modules (Fig. 1B). Modules 1 and 2 are segmentation algorithms for tissue detection and quality control (QC; previously developed and validated GrandQC tool[28]). The QC is a well-validated multiclass algorithm allowing precise exclusion of tissue-containing artifacts from the analysis. In the validation, it showed a Dice score (segmentation accuracy, with 1.0 being ideal segmentation) of 0.938 for detection of nonartificially changed tissue.

Module 3 is a segmentation backbone, developed and extensively clinically validated earlier,[24] which allows pixel-wise segmentation of all relevant tissue classes (n = 11) in colorectal specimens, including all tissue-associated classes: epithelial tumor component, tumor stroma, necrotic debris, mucin, and tertiary lymphoid structures. The algorithm showed a Dice score of 0.88 (average over all classes) in the external validation. For details on segmentation mask postprocessing (module 3) and single-cell mask postprocessing, see Supplementary Methods section.

Extracting Quantitative Parameters

For extraction of quantitative parameters, we split the postprocessed tissue segmentation mask and postprocessed single-cell mask into smaller regions (predefined 1 × 1 mm regions), and the following parameters are saved per region: (1) area of epithelial tumor compartment, (2) area of stromal tumor compartment, (3) number of detected epithelial cells, (4) number of detected lymphocytes in stroma, (5) number of detected lymphocytes in epithelial tumor compartment, (6) number of detected plasma cells in stroma, (7) number of detected neutrophils in stroma, (8) number of detected eosinophils in stroma, and (9) number of detected connective tissue cells in stroma. These per-region outputs are used later for heterogeneity analysis and are also accumulated over the entire slide as a simple sum for slide-level metrics. The details on aggregation from multiple slides and on heatmaps/visualization (Fig. 2A, B) are provided in Supplementary Methods section. All parameters were dichotomized for prognostic analysis. The optimal thresholds were identified systematically (testing thresholds in the form of percentiles of all values in a range P10-P90) in univariate Cox analysis in exploration cohort. After that, thresholds were frozen for validation using external cohorts.

Heterogeneity Analysis

Overlays of binary maps (blue color – below the prognostic threshold; red color – above the prognostic threshold) on original images were generated for all TCGA cases for parameters of

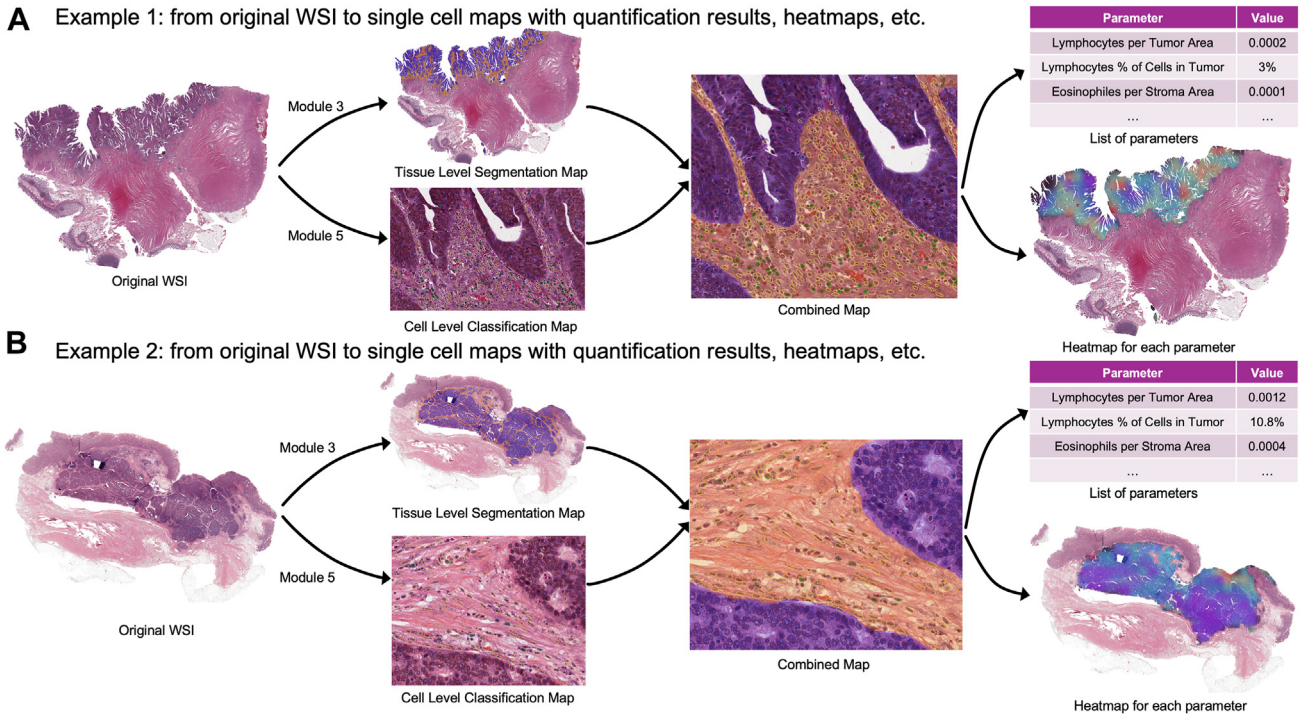

Figure 2.
Examples of whole-slide image processing. The path from original hematoxylin and eosin–stained whole-slide image through multiclass tissue segmentation (with the aim of tumor region detection and segmentation into different compartments: epithelial tumor component, tumor stroma, necrotic debris, mucin, etc.) and single-cell detection and classification. These information layers are then merged and single-cell parameters are extracted in the form of absolute quantifications (number of cells per area) or ratios (percentage of specific cell types in all cells in tumor stroma). The platform allows advanced visualization of all parameters, including heatmaps, enabling full visual control by pathologists. WSI, whole-slide image.

interest. These overlays were analyzed by human analysts to study intratumoral heterogeneity using the following principle: for the superficial part, middle part, and invasion front part of the tumor, the percentage of area over the threshold was determined visually. This assessment was used to study heterogeneity in different compartments of the tumor.

Statistical Analysis

All statistical analyses were performed in R, version 4.0.3 (the R Foundation for Statistical Computing). Descriptive statistics were used to compare clinicopathological variables. Kaplan–Meier estimates with the log-rank test and univariate and multivariate Cox proportional hazards models were implemented to evaluate the prognostic role of extracted parameters.

Code Availability

The code used in the work is available under https://github.com/cpath-ukk/crc_cells/.

Results

Development of Artificial Intelligence Platform for Single-Cell Analysis

The AI-based platform was developed for rigorous characterization of CRC tissue using H&E-stained tissue sections. The platform combines 6 different interconnected modules (Fig. 1B) necessary for extraction of fully quantitative and explainable single cell–based prognostic parameters as well as for the visualization of these biomarkers. The model implements QC steps and uses 2 main deep learning algorithms: (1) a precise multiclass tissue segmentation backbone for colorectal specimens for segmentation of tumor region into different compartments and (2) a single-cell detection/classification algorithm allowing detection of tumor cells, intratumoral stromal and intraepithelial lymphocytes, plasma cells, neutrophilic and eosinophilic granulocytes, and connective tissue cells in different tumor compartments (for examples see Figure 2). We used 3 well-characterized, multi-institutional, digitized cohorts of patient cases with resectable CRC to establish and validate clinically relevant parameters (Fig. 1C, D and Table). The algorithm effectively aggregates from multiple slides for the whole-tumor case and provides visualization maps for each parameter (Fig. 2).

Establishing Single Cell–Based Prognostic Parameters

We used 1 large patient cohort (TCGA) for exploratory purposes and investigated the prognostic role of tumor microenvironment/immune cells. Two main categories of single-cell parameters were established: absolute quantifications (normalized by the compartment area: eg, lymphocytes in stroma) and ratios (ie, percentage of a cell type, eg, neutrophils in stroma). The parameters were quantified at slide level but aggregated to case level for patients with multiple tumor slides available.

In the TCGA cohort, it was shown that each immune cell type, including connective tissue cells and both tumor intraepithelial and stromal lymphocytes, confer significant prognostic value for progression-free survival (PFS) (Fig. 3). For dichotomization based on the best threshold (Fig. 4A), the results of univariate and multivariate analyses (common clinicopathological variables) are

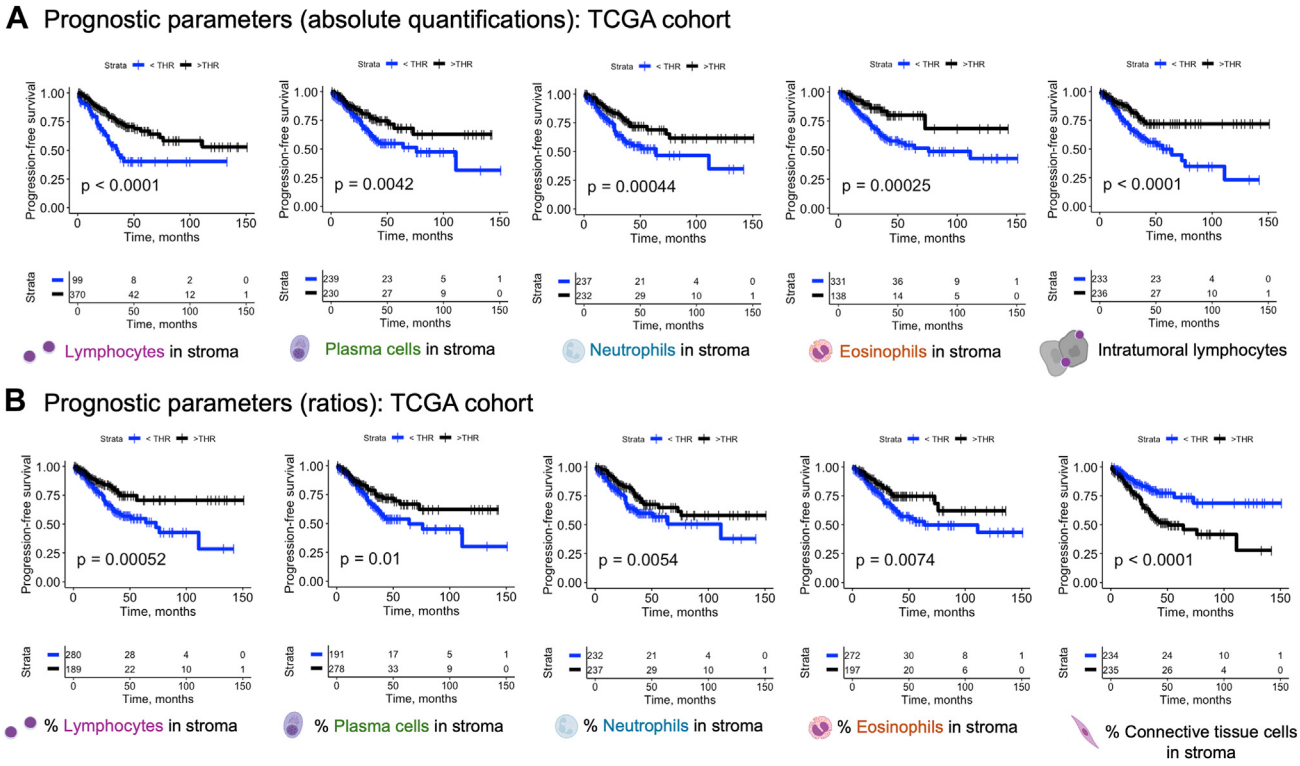

Figure 3.
Prognostic value of single cell type–based parameters. Patient cohort: TCGA (exploratory analysis), progression-free survival as end point. The dichotomization is performed using best identified thresholds. The Kaplan–Meier estimates (*P* values: log-rank test) are presented. The thresholds are provided in Figure 4A. (A) Prognostic parameters based on absolute quantifications (normalized using area). (B) Prognostic parameters based on cell ratios (percentage from the whole number of cells in tumor stroma). TCGA, The Cancer Genome Atlas.

shown in Figure 4A and B, respectively. The analyses revealed that a high percentage of connective tissue cells in stroma is independently associated with worse prognosis, whereas higher normalized absolute quantifications and percentages of all immune cells are independently associated with favorable prognosis (for intercell correlation and correlation with clinicopathological variables, see Supplementary Fig. S1).

Intraepithelial Intratumoral Lymphocytes: Diagnostic and Prognostic Value

Intratumoral lymphocytes (iLYMs) immediately adjacent to tumor cells are a subset of intratumoral tumor-infiltrating lymphocytes (TILs). iLYMs are one of the diagnostic features for detecting high MSI (MSI-H) tumors. Notably, our comparative investigation of iLYM in microsatellite stable (MSS), MSI low (MSI-L), and MSI-H cases (Fig. 4D) shows that although there is a statistical trend to higher iLYM in MSI-H compared with MSS and MSI-L ($P < .001$), many cases in the latter categories show high levels of iLYM. This implies that the latter cannot be used reliably as a diagnostic parameter. Additionally, we showed that in our exploration cohort (TCGA), the prognostic role of iLYM is only evident in MSS/MSI-L patients (Fig. 4D).

Combination Prognostic Parameters

Single cell–based parameters can be complementary and be connected as a compound prognostic system (Fig. 4C, E). First, we systematically built multivariate Cox regression models (PFS) from single parameters and found 4 combinations with statistical significance, all 4 including stromal lymphocytes (absolute quantifications, absolute counts of stromal lymphocytes [abs-sLYMs]) as the core, being the most important prognostic variable (Fig. 4C). In the context of typical clinicopathological variables (pT/pN; other parameters were excluded due to lacking statistical significance in multivariate analysis; for details, see Supplementary Table S1), 2 combinations conferred independent prognostic value: abs-sLYM + stromal neutrophilic granulocyte (absolute quantifications, abs-sNEU) and abs-sLYM + stromal connective tissue cells (percentage, perc-sCON) (Fig. 4E). Both systems allow prognostic stratification of patients into low-, moderate-, and high-risk groups (Fig. 4E). The prognostic value of 1 additional combination, abs-sLYM + abs-sEOS (absolute counts of eosinophils), independently significant in some analyses, is provided in Supplementary Figure S2.

Independent Validation of Single Cell–Based Prognostic Parameters and Systems

Several cohorts were used for validation: 1 well-characterized large cohort (PLCO) of resectable cases containing information on long-term cancer-specific survival (CSS), with other cohorts containing information primarily on overall survival (OS). The PLCO cohort does not contain information about MSI status. First, we showed that all single cell–type prognostic parameters, except stromal plasma cells, retain their prognostic value for CSS in the PLCO cohort (Supplementary Fig. S3, univariate analysis in Fig. 5C; Figs. 6C and 7A). In multivariate analysis, abs-iLYM (HR, 0.62; 95% CI, 0.43-0.89 for high vs low; further details are provided in Fig. 5C), abs-sLYM (HR, 0.67; 95% CI, 0.48-0.94 for high vs low), and

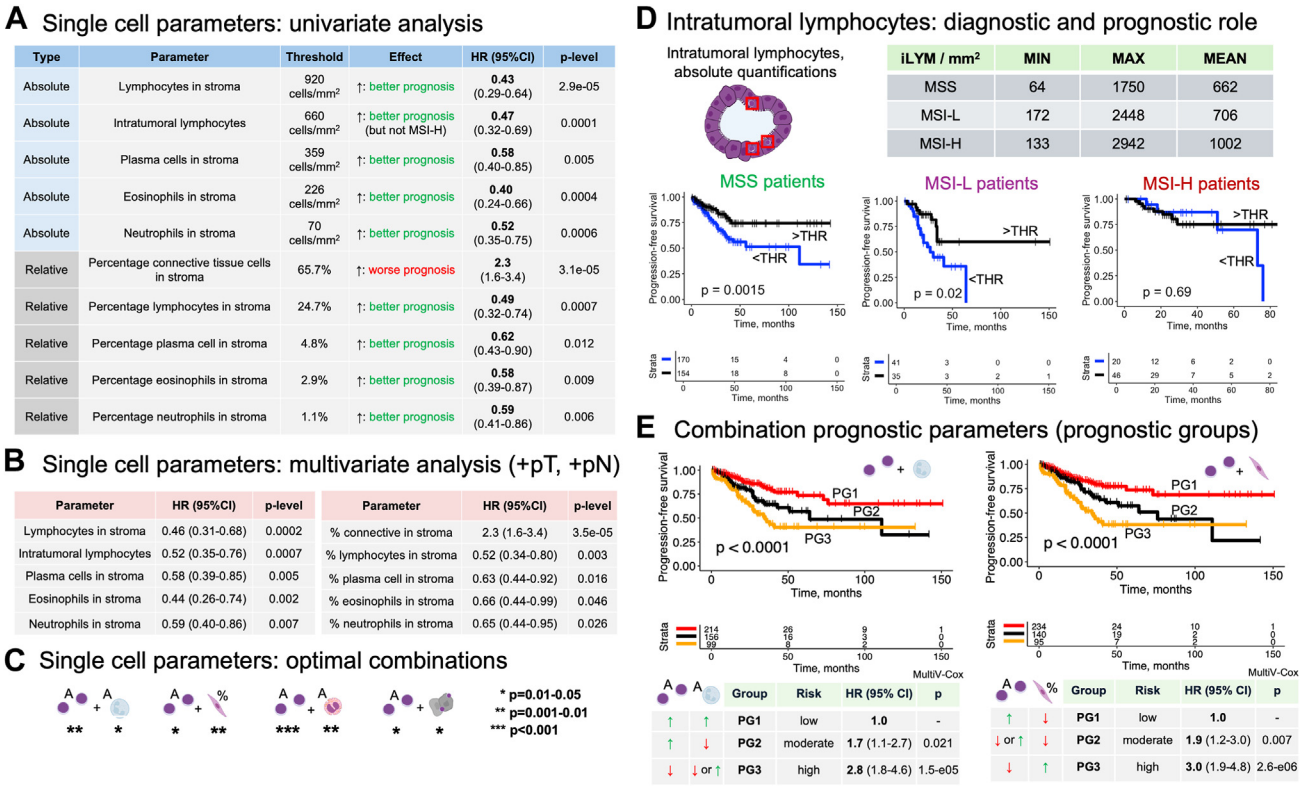

Type	Parameter	Threshold	Effect	HR (95%CI)	p-level
Absolute	Lymphocytes in stroma	920 cells/mm²	↑: better prognosis	**0.43** (0.29-0.64)	2.9e-05
Absolute	Intratumoral lymphocytes	660 cells/mm²	↑: better prognosis (but not MSI-H)	**0.47** (0.32-0.69)	0.0001
Absolute	Plasma cells in stroma	359 cells/mm²	↑: better prognosis	**0.58** (0.40-0.85)	0.005
Absolute	Eosinophils in stroma	226 cells/mm²	↑: better prognosis	**0.40** (0.24-0.66)	0.0004
Absolute	Neutrophils in stroma	70 cells/mm²	↑: better prognosis	**0.52** (0.35-0.75)	0.0006
Relative	Percentage connective tissue cells in stroma	65.7%	↑: worse prognosis	**2.3** (1.6-3.4)	3.1e-05
Relative	Percentage lymphocytes in stroma	24.7%	↑: better prognosis	**0.49** (0.32-0.74)	0.0007
Relative	Percentage plasma cell in stroma	4.8%	↑: better prognosis	**0.62** (0.43-0.90)	0.012
Relative	Percentage eosinophils in stroma	2.9%	↑: better prognosis	**0.58** (0.39-0.87)	0.009
Relative	Percentage neutrophils in stroma	1.1%	↑: better prognosis	**0.59** (0.41-0.86)	0.006

Parameter	HR (95%CI)	p-level	Parameter	HR (95%CI)	p-level
Lymphocytes in stroma	0.46 (0.31-0.68)	0.0002	% connective in stroma	2.3 (1.6-3.4)	3.5e-05
Intratumoral lymphocytes	0.52 (0.35-0.76)	0.0007	% lymphocytes in stroma	0.52 (0.34-0.80)	0.003
Plasma cells in stroma	0.58 (0.39-0.85)	0.005	% plasma cell in stroma	0.63 (0.44-0.92)	0.016
Eosinophils in stroma	0.44 (0.26-0.74)	0.002	% eosinophils in stroma	0.66 (0.44-0.99)	0.046
Neutrophils in stroma	0.59 (0.40-0.86)	0.007	% neutrophils in stroma	0.65 (0.44-0.95)	0.026

iLYM / mm²	MIN	MAX	MEAN
MSS	64	1750	662
MSI-L	172	2448	706
MSI-H	133	2942	1002

Group	Risk	HR (95% CI)	p
PG1	low	**1.0**	-
PG2	moderate	**1.7** (1.1-2.7)	0.021
PG3	high	**2.8** (1.8-4.6)	1.5-e05

Group	Risk	HR (95% CI)	p
PG1	low	**1.0**	-
PG2	moderate	**1.9** (1.2-3.0)	0.007
PG3	high	**3.0** (1.9-4.8)	2.6-e06

Figure 4.
Advanced prognostic analysis of single cell–based parameters and their combinations in the exploration cohort (TCGA cohort). (A) Univariate analysis using progression-free survival as end point. The thresholds used are provided. Higher numbers of all cells, except for connective tissue cells, are associated with better prognosis for both absolute and relative (ratios) measurements, whereas a higher percentage of connective tissue cells is associated with worse prognosis. (B) Multivariate analysis with inclusion of pT and pN pathological variables. All parameters show independent prognostic value. (C) Combinations of single-cell parameters showing complementary prognostic value. Statistical significance levels presented are from systematic multivariate Cox analysis of different combinations, including only single-cell parameters (without clinicopathological variables). (D) Diagnostic and prognostic role of intraepithelial intratumoral lymphocytes (iLYM, absolute counts normalized by tumor tissue area). Intraepithelial lymphocytes are considered a diagnostic feature of MSI-H tumors. Our analysis shows that MSS and MSI-L tumors show high levels of iLYM on a regular basis, precluding use of this parameter for diagnostic purposes. Prognostic role of iLYM is prominent but conferred only to MSS/MSI-L patients. (E) Analysis of combination of prognostic parameters, resulting in prognostic systems. Stromal intratumoral lymphocytes + neutrophils (both absolute counts) as well as stromal intratumoral lymphocytes (absolute) + connective tissue cells (relative/percentage) allow potent patient stratification according to progression risk into low-, intermediate-, and high-risk groups. All hazard ratios and *P* levels are from multivariate Cox analysis including pT and pN categories of the tumor. HR, hazard ratio; MAX, maximal value; MIN, minimal value; MSI-H, high microsatellite instability; MSI-L, low microsatellite instability; MSS, microsatellite stability; THR, threshold.

abs-sNEU (HR, 0.59; 95% CI, 0.40-0.88 for high vs low) showed independent prognostic value for the CSS end point. For OS end point, 7 of 10 parameters showed independent prognostic value in a large merged cohort (TCGA + PLCO + FED-PATH; Supplementary Fig. S4A). Prognostic analysis for single cell–based parameters in a smaller FED-PATH cohort (PFS as the end point) and for the merged cohort (OS as the end point) is provided in Supplementary Figures S5 and S6, showing results similar to those of the PLCO and TCGA cohorts, as already described here.

As for prognostic systems, abs-sLYM + abs-sNEU showed independent prognostic value clearly for CSS end points and with small but statistically significant differences in multivariate analysis for OS end points (Fig. 5A, D). For the abs-sLYM + perc-sCON system, only the high-risk group was an independent predictor for CSS in multivariate analysis (Fig. 5B; analysis of other combinations for the merged cohort/OS in Supplementary Fig. S4B, C).

Intratumoral Heterogeneity of Single Cell–Based Prognostic Parameters

The developed platform allows visualization of single-cell parameter measurements for investigation of the intratumoral heterogeneity (Fig. 5E). Importantly, when visualized on the regional level (~1 × 1 mm), all parameters showed significant heterogeneity that might be important for clinical decision making. In 1 large cohort (TCGA), we performed semiquantitative assessment of intratumoral heterogeneity for 5 parameters with independent prognostic value (Fig. 6A). For each slide, based on the morphologic context, the percentage of area positive for the parameter (>prognostic threshold, as in Fig. 4A) was estimated for tumor surface, middle region, and invasion front (if available in slide). Next, all cases were split into “high” or “low” prognostic groups based on single prognostic parameters (as in Fig. 4A). Some important findings are evident. Thus, even in abs-sLYM “low” cases, on average 72% of the tumor surface showed “high” levels of abs-sLYM, probably due to activation through intestinal content/bacteria. However, in general, in “high" cases for all parameters, independent of compartment, the dominant part of the tumor showed regionally high parameter levels (Fig. 6A).

Applicability of Parameters to Biopsy Samples

Prognostication based on the analysis of tumor biopsy samples provides additional clinical value. We applied our platform to

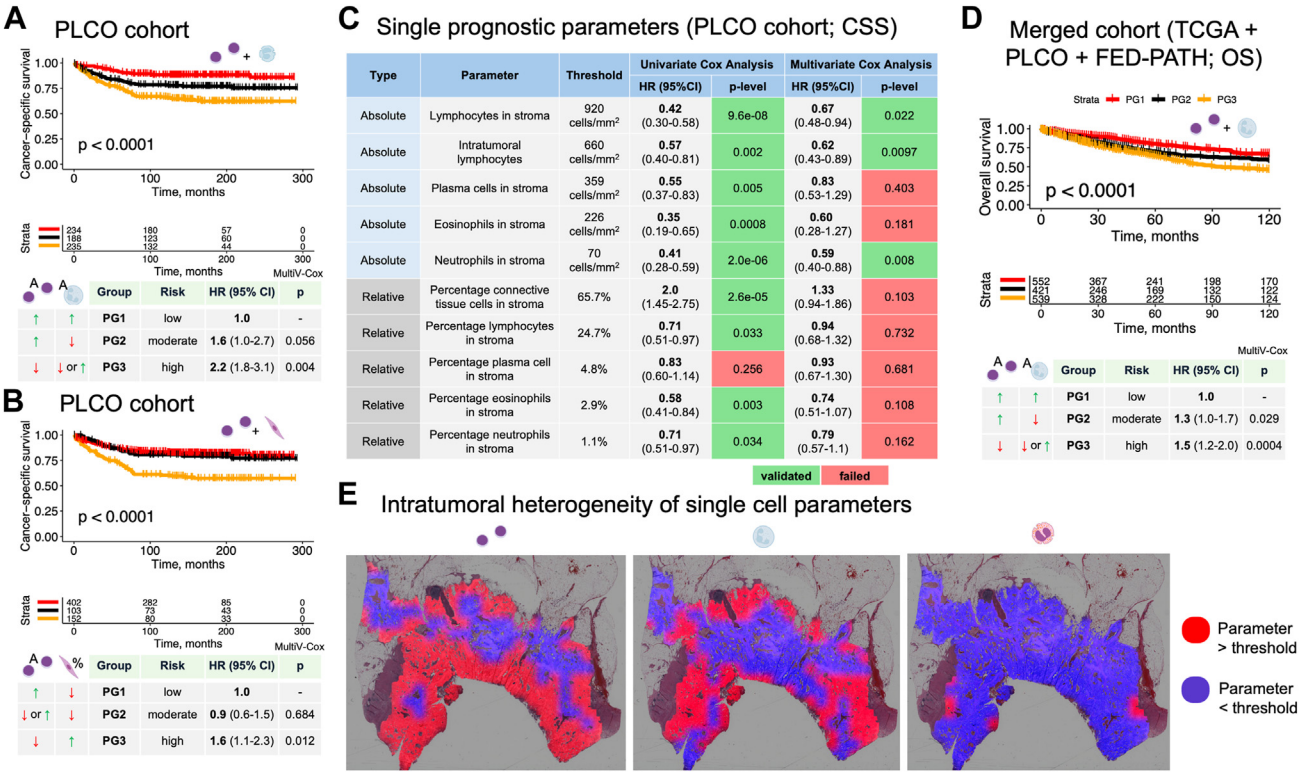

Figure 5.
Independent validation of single cell–based prognostic parameters/prognostic systems and intratumoral heterogeneity of the single-cell parameters. (A) Prognostic system: stromal intratumoral lymphocytes + neutrophils (both absolute counts). Patient cohort: PLCO. clinical endpoint: cancer-specific survival. (B) Prognostic system: stromal intratumoral lymphocytes (absolute) + connective tissue cells (relative/percentage). Patient cohort: PLCO. Clinical endpoint: cancer-specific survival. (C) Univariate and multivariate analysis in PLCO cohort using cancer-specific survival as endpoint. The thresholds used are the same as in the exploration cohort. (D) Prognostic system: stromal intratumoral lymphocytes + neutrophils (both absolute counts). Patient cohort: merged − 3 study cohorts. Clinical end point: overall survival. (E) Significant intratumoral heterogeneity for all single-cell parameters can be observed. Red color: parameter value above threshold (same thresholds as in Figures 4A and 6C), blue color: parameter value below threshold. Detailed quantitative evaluation according to different tumor compartments is provided in Figure 7A. CSS, cancer-specific survival; HR, hazard ratio; OS, overall survival; PLCO, Prostate, Lung, Colorectal, and Ovarian Cancer Screening Trial; TCGA, The Cancer Genome Atlas.

whole-slide images of 1 biopsy case cohort (cases n = 61). We used pN+ status at resection or diagnosis of synchronous distant metastasis (M1syn) as a surrogate for disease progression and negative clinical outcome. The results separated by pN+/M1syn and pN0/M0syn are provided in Figure 6B. In this limited-size cohort, we found that the constellation of "low" abs-sLYM and "low" abs-sNEU in the biopsy carried substantially higher risk (~3× higher risk) of pN+/M1syn.

"Out-of-Control" Tumor Area: Tumor Biology and Prognostic Implications

During morphologic analysis of intratumoral heterogeneity maps, an important finding was recognized: the regions with low levels of intraepithelial intratumoral lymphocytes frequently co-occurred with high levels of connective tissue cells in stroma and vice versa (Fig. 6C). This biological mechanism has been described previously with cancer-associated fibroblasts preventing access of T cells to tumor cells (see Discussion section for further analysis).

Our platform allows for fully quantitative assessment of such regions, and we hypothesized that tumor proportion where the tumor is "out of control" of the immune system (low abs-iLYM/high perc-sCON) is mirroring aggressive tumor biology features and should have prognostic implications. Importantly, for the PFS end point in the TCGA cohort, there is a clear prognostic stratification based on the percentage of tumor "out of control." Subcohorts of patients, of substantial size, can be identified: with very good prognosis (area "out of control" < 10%) and at very high risk of progression (area > 60%; multivariate HR, 5.2; $P = 2e\text{-}05$) (Fig. 6D). We have also shown that area "out of control" is highly correlated with pN+ status, postoperative disease progression, and development of distant metastasis (Fig. 6D).

Of interest, in all MSI-H tumors, an average of 12.3% of the whole-tumor area is "out of control," with MSS/MSI-L tumors having on average of >40% of the tumor not controlled by the immune system. This provides an additional insight into tumor biology of MSI/MSS cancers and offers clarification on their differing clinical aggressivity profiles (Fig. 6D).

These findings were validated in multivariate analysis in the PLCO cohort using a CSS end point (Fig. 7) and for patient subgroups with limited nodal disease (pN1) and pN0. Notably, using 5% as a cutoff of area "out of control" provided even better identification of PLCO patients with excellent prognosis compared with TCGA. Most patients from the PLCO cohort had more than 1 tumor slide available (Fig. 1D; for most TCGA patients, only 1 slide with potential selection bias), rendering this cohort as potentially more representative.

Discussion

In this study, we developed a quantitative AI-based platform for tissue analysis in patients with resectable CRC (Figs. 1A, B and 2)

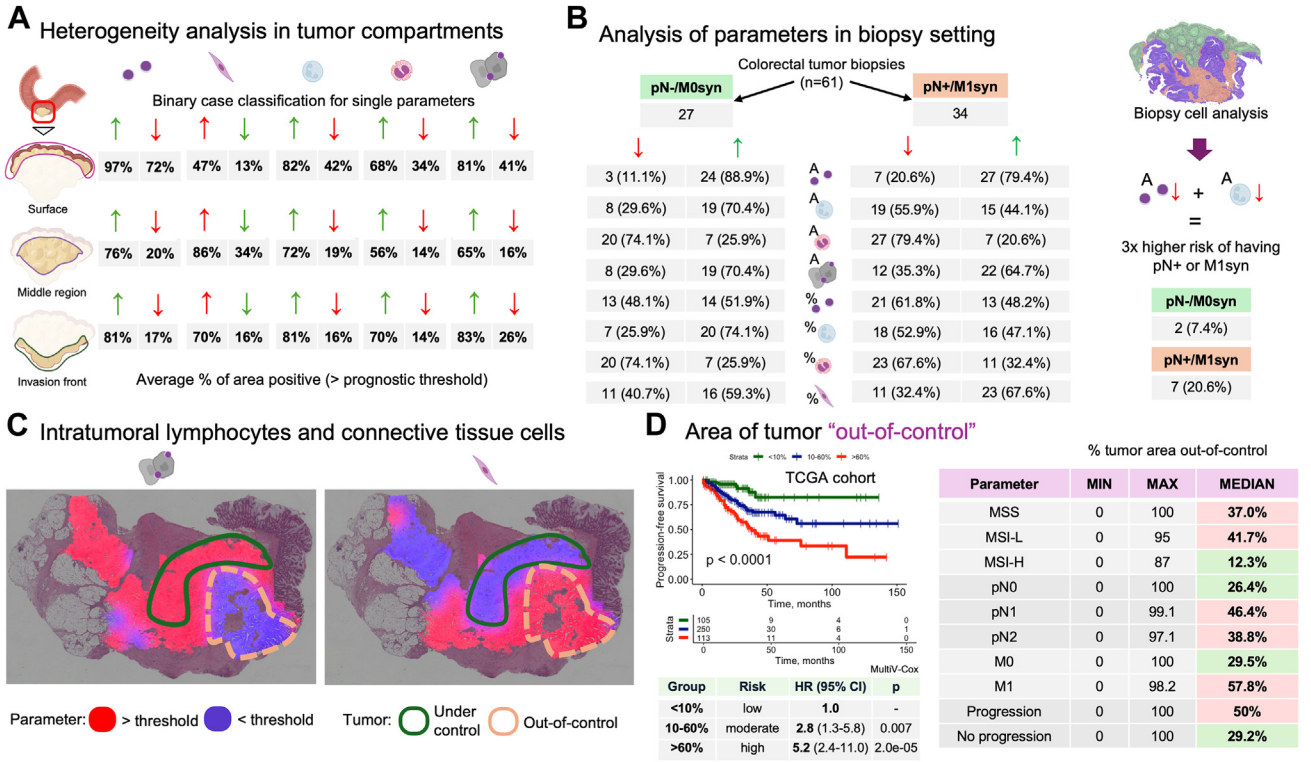

Figure 6.

Intratumoral heterogeneity of single cell–based parameters in different tumor compartments, analysis of biopsy samples, and area of tumor "out-of-control" concept and prognostic parameter. (A) Single cell–based parameters demonstrate significant intratumoral heterogeneity. A detailed investigation of intratumoral heterogeneity was performed for all new parameters assessing normalized absolute values of different cell populations. For this, first, all cases (TCGA cohort) were classified as "high" and "low" for each single parameter (using established thresholds, see Fig. 4A). Second, for each case and each parameter the visual maps were produced (examples in Fig. 6E; "red" = region within tumor with parameter value higher than threshold, "blue" – lower than threshold). Next, human analysts estimated the percentage of "red" areas in all cases, separately in different tumor compartments (surface, middle region, invasion front). The rates of positivity for single parameters are summarized, separately for cases with "high" and "low" status showing significant heterogeneity. This might have implications for testing of parameters in the biopsy setting, eg, stromal lymphocyte "low" cases can show high stromal lymphocyte counts on the tumor surface, presumably related to the activation via bacteria and luminal intestinal content. Eosinophils and intratumoral intraepithelial lymphocytes tend to be underrepresented in tumor middle regions in cases classified as "high" for these parameters. (B) Analysis of single cell–based parameters in a cohort of biopsy tumor samples (n = 61). No prognostic information is available for these cases and pN+ status at resection or synchronous M1 status are used as surrogate for progression risk/negative clinical outcome. Biopsy samples "low" for both stromal intratumoral lymphocytes and neutrophilic granulocytes might be predictive for pN+/M1syn in biopsy setting (~×3 higher risk when both parameters are "low"/under threshold). (C) Morphologic analysis of intratumoral heterogeneity revealed an important constellation/concept. In many regions, low levels of intratumoral intraepithelial lymphocytes are correlated with an increased number of connective tissue cells (morphologically fibroblasts) in tumor stroma. Cancer-associated fibroblasts are believed to restrict access of lymphocytes to tumor cells, however, this might be a consequence of tumor cells escaping from immune system control. We hypothesize that these are the regions where the tumor is "out-of-control" of the immune system – aggressivity hotspots that should influence the disease outcome. Quantitative assessment of tumor area (% of area) "out of control" is an independent prognostic parameter. Kaplan–Meier estimates (log-rank test for *P* value; progression-free survival; TCGA cohort) are shown for trichotomization using cutoffs <10% of tumor area "out of control," 10% to 60%, and >60% with the former defining large subgroup of patients with excellent prognosis and the latter a large subgroup of patients with poor prognosis. The hazard ratios and *P* levels presented in the table stem from multivariate Cox analysis with inclusion of pT and pN categories. Table on the right side: Substantially larger areas (%) of tumor "out of control" are evident in MSS/MSI-L cases, pN+ cases, progression cases, and cases that developed M1 in the course of the disease. These findings were validated in the independent PLCO cohort (Supplementary Fig. S4A-C) including patient subgroups with limited nodal disease (Supplementary Fig. S4D) and pN0 (Supplementary Fig. S4E). HR, hazard ratio; M0syn/M1syn, synchronous distant metastasis; MSI-H, high microsatellite instability; MSI-L, low microsatellite instability; MSS, microsatellite stability; TCGA, The Cancer Genome Atlas.

that can serve as a capable extractor of explainable prognostic information from conventional H&E-stained tissue sections. It addresses 2 critical clinical gaps. (1) The lack of automated, explainable, and objective biomarkers, which can improve clinical staging and navigate important life-prolonging decisions (such as the necessity of adjuvant therapy after resection). (2) The ability to measure and understand immune-evasion mechanisms, which contribute to tumor aggressiveness. A key innovation is the "out-of-control" tumor area—a biomarker highlighting regions where tumors escape immune surveillance. This, along with stromal lymphocyte and neutrophil counts, allows for stratification of patients into risk groups and demonstrates independent prognostic value in external validation (Fig. 6A-D). Developed instrument performs analysis on routine immunohistochemistry sections and does not require additional stains (eg, for ImmunoScore analysis[3,4]).

Only 1 previous study, by Vayrynen et al,[23] linked stromal immune cell densities to prognosis in CRC but relied on tissue microarrays from central tumor regions, which can introduce selection bias and fail to capture tumor heterogeneity. In contrast, our study analyzed full-slide images across multiple cohorts, providing a more comprehensive view of the tumor microenvironment. By using state-of-the-art machine learning for tissue segmentation and single-cell classification, our method avoids the limitations of handcrafted features and ensures greater generalizability. Our findings highlight significant intratumoral variation in immune cell distribution, emphasizing the need for whole-tumor assessment to improve prognostic accuracy

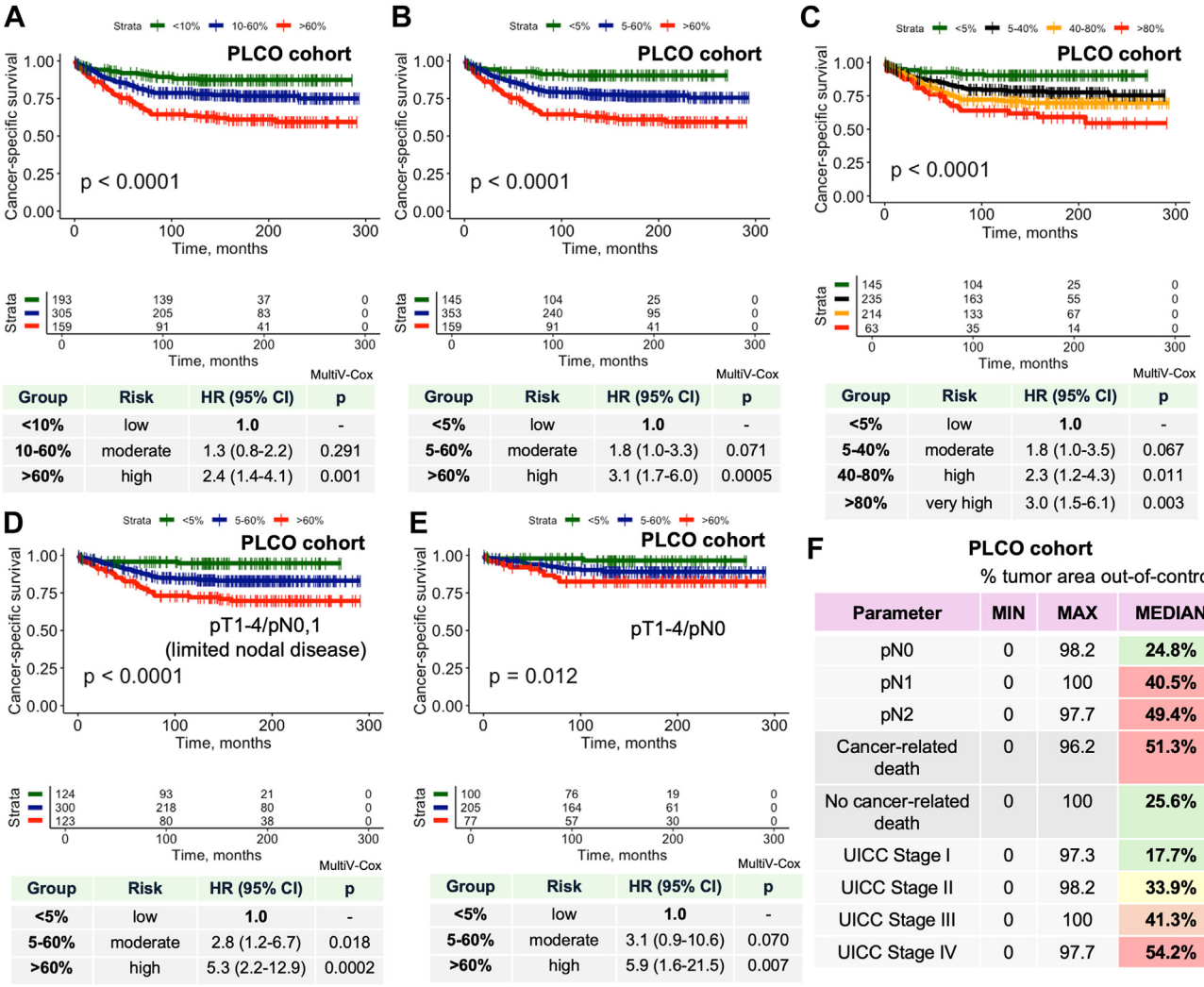

Figure 7.
Quantitative assessment of tumor area (% of area) "out of control" as a prognostic parameter in the PLCO cohort. (A-E) Kaplan–Meier estimates (log-rank test for *P* value; cancer-specific survival) are shown using different cutoffs: (A) Three prognostic groups: <10% of tumor area "out of control," 10% to 60%, and >60% with the former defining large subgroup of patients with excellent prognosis and the latter a large subgroup of patients with poor prognosis. (B) Three prognostic groups: <5%, 5% to 60%, and >60%. (C) Four prognostic groups: <5%, 5% to 40%, 40% to 80%, and >80%. (D) Same as B for pT1-4/pN0-1 subcohort (limited nodal disease), (E) same as B for pT1-4/pN0 subcohort. Comment: The hazard ratios (HRs) and *P* levels presented in the table stem from multivariate Cox analysis with inclusion of pT and pN categories. (F) Substantially larger areas (%) of tumor "out of control" are evident in microsatellite stability/low microsatellite instability cases, pN+ cases, in cases with cancer-related death, and cases with higher UICC Stage. MAX, maximal value; MIN, minimal value; PLCO, Prostate, Lung, Colorectal, and Ovarian Cancer Screening Trial; UICC, Union for International Cancer Control.

(Figs. 5E and 6A). Interestingly, Vayrynen et al[23] analyzed intraepithelial plasma cells and neutrophilic and eosinophilic granulocytes. In our examination, most neutrophilic and eosinophilic granulocytes were found in the context of luminal necrosis, and plasma cells were absent in the intraepithelial compartment. Vayrynen et al[23] and our study come to similar conclusions regarding prognostic parameters.

Our analysis identified the "out-of-control" tumor area—regions with low intratumoral lymphocytes and increased connective tissue cells (most of them being fibroblasts during visual evaluation by pathologists) highlighting aggressive tumor behavior. Cancer-associated fibroblasts (CAFs) within these regions may contribute to immune evasion, a factor linked to unfavorable outcomes in CRC.[29,30] The presumable mechanism is that CAFs block access of lymphocytes to the tumor cells; however, it is not clear if CAF expansion is a cause or just a consequence of tumor cells escaping from immune control in the first place.[31,32]

The "out-of-control" biomarker independently stratifies patients by prognosis, including those with limited or absent nodal disease metastasis (Figs. 6D and 7). To the best of our knowledge, this is the first conceptual description and AI-based implementation of the "out-of-control" tumor area parameter using regular H&E slides.

Several other studies used deep learning for analysis of prognostic stratification in CRC but most focus on either specific cell types or tissue features in isolation.[7-22] As for the explainable quantitative approach, in a series of well-planned development and validation studies, Pai et al[20-22] created a QuantCRC tool that requires manual tumor region selection and primarily assesses 1 cellular parameter (density of intraepithelial lymphocytes/TIL).[22] In our study, we not only demonstrated a fully automized analysis but also performed a detailed investigation of a multitude of cell types and parameters, including TILs. Importantly, in our study, distinct from most previous reports[21,33-35] and given precise

segmentation maps of the tumor region, we were able to subclassify TILs into iLYM (intraepithelial intratumoral lymphocytes) and sLYM (stromal intratumoral lymphocytes). We provide evidence that in CRC these 2 fractions might carry slightly different prognostic value, with iLYMs lacking prognostic significance in MSI cases (TCGA cohort; Fig. 4C). This warrants further investigation of these 2 fractions separately.

Among explainable analytical tools, Bokhorst et al[13] developed a fully automated prognostic tool for tumor bud assessment, which, similar to QuantCRC by Pai et al,[22] showed independent prognostic value. Jiao et al,[36] Kather et al,[17] Liu et al,[12] and Xu et al[16] used tissue (stroma)-related features and/or intratumoral lymphocytes (different definitions) from less-precise patch-level tissue.[22] Although Graham et al[37] presented an appealing view on how multiple tasks (tissue segmentation and cell segmentation) can be unified into 1 algorithm, they do not investigate their tool in prognostic applications. Using multiple algorithms (Pai et al,[21] Bokhorst et al,[13] Vayrynen et al,[23] and our own platform) is not a limitation but can reduce computational effort. Several studies[7,8,11,14] utilized an end-to-end approach, with Jiang et al[8] showing that convolutional neural networks can extract information directly from images without supervision (using RetCCL[38]).[39] Similar approaches exist[7,11,14,18]; however, these methods have limited interpretability/explainability, although single biomarkers stemming from the studies did evolve into explainable image features (such as tumor-adipose feature[18,40] or the non−AI-based SARIFA biomarker[41]), under extensive validation currently.

Our study is not devoid of limitations. First, it uses retrospective cohorts, and prospective validation is necessary. Second, more detailed studies of the prognostic role of new parameters are necessary in MSI/MSS subgroups of patients with CRC. MSI status was not available on FED-PATH or PLCO cohorts, which represents a limitation of these data sets. Third, the “connective tissue” cell class, defined by the cell segmentation algorithm used, is a collective term for several cell types including not only fibroblasts but also endothelial cells, and, importantly, histiocytes. More fine granular stratification of connective tissue cells might be necessary, which is not possible with the current version of the algorithm and is a subject of further research. Finally, integral evaluations are lacking and highly warranted to bring the markers examined together within a single study, allowing a clear understanding of their interdependencies.

Acknowledgments

The authors thank the Regional Computing Center of the University of Cologne (RRZK) for providing computing time on the DFG-funded (Funding number: INST 216/512/1FUGG) High-Performance Computing (HPC) system CHEOPS as well as technical support.

Author Contributions

V.M.B. contributed to algorithm training, pipeline development, data management, data analysis and interpretation, pathological analysis, statistical analysis, and manuscript drafting. Z.W. performed data analysis and technical implementation of pipeline. L.G., M.B., and C.W. contributed to data management and analysis. R.B. contributed to supervision, data management, and resources. A.Q. and T.Z. contributed to data management, data analysis, and resources. Y.T. contributed to conception and study design, algorithm training, pipeline development, data management, data analysis and interpretation, statistical analysis, manuscript drafting, resources, and supervision. All authors: critical revision for important intellectual context. All authors read and approved the final version of the paper.

Data Availability

TCGA and PLCO data sets are available online. The code of algorithm for parameter extraction and quantification will be released at GitHub upon publication. The authors open-source fully anonymized FED-PATH data set (UKK subset; whole-slide images, cell detections, clinical/follow-up data) for academic research (upon publication). The code used in the work is deposited under https://github.com/cpath-ukk/crc_cells.

Funding

This project was funded by Federal Ministry of Education and Research of Germany: Project FED-PATH (Y.T., Z.W., R.B., and C.W.), InterReg EU/EFRE program: Project DigiPathConnect (Y.T. and R.B.), and by North Rhine-Westphalia state (European Fond for Regional Development (EFRE), 2014-2020; REACT-EU): Project DIGI-PATH (Y.T. and R.B.). Y.T. and V.B. had access to all the data.

Declaration of Competing Interest

All authors report no relevant conflicts of interest related to this study.

Ethics Approval and Consent to Participate

All study steps were performed in accordance with the Declaration of Helsinki. This study was approved by the Ethical committee of the University of Cologne (20-1583), Halle/Cologne joint 22-1233 (Project FED-PATH). Given the retrospective/archive nature of used data, the necessity of obtaining patients' permission was waived by the ethical committee.

Declaration of Generative AI and AI-Assisted Technologies in the Writing Process

During the preparation of this work the author(s) used Grammarly and ChatGPT to improve readability and language. After using this tool/service, the authors reviewed and edited the content as needed and take full responsibility for the content of the publication.

Supplementary Material

The online version contains supplementary material available at https://doi.org/10.1016/j.modpat.2025.100771.

References

1. Morgan E, Arnold M, Gini A, et al. Global burden of colorectal cancer in 2020 and 2040: incidence and mortality estimates from GLOBOCAN. *Gut*. 2023;72(2):338−344. https://doi.org/10.1136/GUTJNL-2022-327736
2. WHO Classification of Tumours Editorial Board. *Digestive System Tumours WHO Classification of Tumours*. 5th ed. IARC, WHO; 2019.
3. Pagès F, Mlecnik B, Marliot F, et al. International validation of the consensus Immunoscore for the classification of colon cancer: a prognostic and accuracy study. *Lancet*. 2018;391(10135):2128−2139. https://doi.org/10.1016/S0140-6736(18)30789-X

4. Galon J, Costes A, Sanchez-Cabo F, et al. Type, density, and location of immune cells within human colorectal tumors predict clinical outcome. *Science*. 2006;313(5795):1960–1964. https://doi.org/10.1126/SCIENCE.1129139
5. Bera K, Schalper KA, Rimm DL, Velcheti V, Madabhushi A. Artificial intelligence in digital pathology—new tools for diagnosis and precision oncology. *Nat Rev Clin Oncol*. 2019;16(11):703–715. https://doi.org/10.1038/s41571-019-0252-y
6. Echle A, Rindtorff NT, Brinker TJ, Luedde T, Pearson AT, Kather JN. Deep learning in cancer pathology: a new generation of clinical biomarkers. *Br J Cancer*. 2021;124(4):686–696. https://doi.org/10.1038/S41416-020-01122-X
7. Höhn J, Krieghoff-Henning E, Wies C, et al. Colorectal cancer risk stratification on histological slides based on survival curves predicted by deep learning. *NPJ Precis Oncol*. 2023;7(1):98. https://doi.org/10.1038/s41698-023-00451-3
8. Jiang X, Hoffmeister M, Brenner H, et al. End-to-end prognostication in colorectal cancer by deep learning: a retrospective, multicentre study. *Lancet Digit Health*. 2024;6(1):e33–e43. https://doi.org/10.1016/S2589-7500(23)00208-X
9. Yang J, Ye H, Fan X, et al. Artificial intelligence for quantifying immune infiltrates interacting with stroma in colorectal cancer. *J Transl Med*. 2022;20(1):1–11. https://doi.org/10.1186/S12967-022-03666-3/FIGURES/4
10. Sinicrope FA, Nelson GD, Saberzadeh-Ardestani B, et al. Use of deep learning to evaluate tumor microenvironmental features for prediction of colon cancer recurrence. *Cancer Res Commun*. 2024;4(5):1344–1350. https://doi.org/10.1158/2767-9764.CRC-24-0031
11. Zhou J, Foroughi pour A, Deirawan H, et al. Integrative deep learning analysis improves colon adenocarcinoma patient stratification at risk for mortality. *EBioMedicine*. 2023;94:104726. https://doi.org/10.1016/j.ebiom.2023.104726
12. Liu A, Li X, Wu H, et al. Prognostic significance of tumor-infiltrating lymphocytes using deep learning on pathology images in colorectal cancers. *JCO Precis Oncol*. 2023;7:e2200522. https://doi.org/10.1200/PO.22.00522
13. Bokhorst JM, Ciompi F, Öztürk SK, et al. Fully automated tumor bud assessment in hematoxylin and eosin-stained whole slide images of colorectal cancer. *Mod Pathol*. 2023;36(9):100233. https://doi.org/10.1016/J.MODPAT.2023.100233
14. Bychkov D, Linder N, Turkki R, et al. Deep learning based tissue analysis predicts outcome in colorectal cancer. *Sci Rep*. 2018;8(1):3395. https://doi.org/10.1038/s41598-018-21758-3
15. Xu H, Cha YJ, Clemenceau JR, et al. Spatial analysis of tumor-infiltrating lymphocytes in histological sections using deep learning techniques predicts survival in colorectal carcinoma. *J Pathol Clin Res*. 2022;8(4):327–339. https://doi.org/10.1002/CJP2.273
16. Xu Z, Li Y, Wang Y, et al. A deep learning quantified stroma-immune score to predict survival of patients with stage II-III colorectal cancer. *Cancer Cell Int*. 2021;21(1):1–12. https://doi.org/10.1186/S12935-021-02297-W/FIGURES/5
17. Kather JN, Krisam J, Charoentong P, et al. Predicting survival from colorectal cancer histology slides using deep learning: a retrospective multicenter study. *PLoS Med*. 2019;16(1):e1002730. https://doi.org/10.1371/JOURNAL.PMED.1002730
18. Wulczyn E, Steiner DF, Moran M, et al. Interpretable survival prediction for colorectal cancer using deep learning. *npj Digit Med*. 2021;4(1):71. https://doi.org/10.1038/s41746-021-00427-2
19. Pai R, Wu C, Kosiorek HE, et al. Development of an improved risk stratification scheme for stage II and III colorectal cancers through incorporation of the digital pathology biomarker QuantCRC. *J Clin Oncol*. 2024;42(3_suppl). https://doi.org/10.1200/JCO.2024.42.3_SUPPL.162
20. Wu C, Pai RK, Kosiorek H, et al. Improved risk-stratification scheme for mismatch-repair proficient stage II colorectal cancers using the digital pathology biomarker QuantCRC. *Clin Cancer Res*. 2024;30(9):1811–1820. https://doi.org/10.1158/1078-0432.CCR-23-3211
21. Pai RK, Hartman D, Schaeffer DF, et al. Development and initial validation of a deep learning algorithm to quantify histological features in colorectal carcinoma including tumour budding/poorly differentiated clusters. *Histopathology*. 2021;79(3):391–405. https://doi.org/10.1111/HIS.14353
22. Pai RK, Banerjee I, Shivji S, et al. Quantitative pathologic analysis of digitized images of colorectal carcinoma improves prediction of recurrence-free survival. *Gastroenterology*. 2022;163(6):1531–1546.e8. https://doi.org/10.1053/j.gastro.2022.08.025
23. Vayrynen JP, Lau MC, Haruki K, et al. Prognostic significance of immune cell populations identified by machine learning in colorectal cancer using routine hematoxylin and eosin-stained sections. *Clin Cancer Res*. 2020;26(16):4326–4338. https://doi.org/10.1158/1078-0432.CCR-20-0071
24. Griem J, Eich ML, Schallenberg S, et al. Artificial intelligence-based tool for tumor detection and quantitative tissue analysis in colorectal specimens. *Mod Pathol*. 2023;36(12):100327. https://doi.org/10.1016/J.MODPAT.2023.100327
25. Schmidt U, Weigert M, Broaddus C, Myers G. Cell detection with star-convex polygons. In: Frangi A, Schnabel J, Davatzikos C, Alberola-López C, Fichtinger G, eds. *Medical Image Computing and Computer Assisted Intervention – MICCAI 2018. MICCAI 2018*. Cham: Springer Intl; 2018:265–273. https://doi.org/10.1007/978-3-030-00934-2_30
26. Graham S, Vu QD, Jahanifar M, et al. CoNIC challenge: pushing the frontiers of nuclear detection, segmentation, classification and counting. *Med Image Anal*. 2024;92:103047. https://doi.org/10.1016/J.MEDIA.2023.103047
27. Graham S, Jahanifar M, Azam A, et al. *Lizard: a large-scale dataset for colonic nuclear instance segmentation and classification. Proceedings of the IEEE International Conference on Computer Vision*. IEEE; 2021:684–693. https://doi.org/10.1109/ICCVW54120.2021.00082
28. Weng Z, Seper A, Pryalukhin A, et al. GrandQC: a comprehensive solution to quality control problem in digital pathology. *Nat Commun*. 2024;15(1):10685. https://doi.org/10.1038/S41467-024-54769-Y
29. Chen YF, Yu ZL, Lv MY, et al. Cancer-associated fibroblasts impact the clinical outcome and treatment response in colorectal cancer via immune system modulation: a comprehensive genome-wide analysis. *Mol Med*. 2021;27(1):139. https://doi.org/10.1186/S10020-021-00402-3
30. Tommelein J, Verset L, Boterberg T, Demetter P, Bracke M, De Wever O. Cancer-associated fibroblasts connect metastasispromoting communication in colorectal cancer. *Front Oncol*. 2015;5:63. https://doi.org/10.3389/FONC.2015.00063
31. Baker AT, Abuwarwar MH, Poly L, Wilkins S, Fletcher AL. Cancer-associated fibroblasts and T cells: from mechanisms to outcomes. *J Immunol*. 2021;206(2):310–320. https://doi.org/10.4049/JIMMUNOL.2001203
32. Sahai E, Astsaturov I, Cukierman E, et al. A framework for advancing our understanding of cancer-associated fibroblasts. *Nat Rev Cancer*. 2020;20(3):174–186. https://doi.org/10.1038/s41568-019-0238-1
33. Millward J, He Z, Nibali A, et al. Automated deep learning-based assessment of tumour-infiltrating lymphocyte density determines prognosis in colorectal cancer. *J Transl Med*. 2025;23(1):1–14. https://doi.org/10.1186/S12967-025-06254-3
34. Thagaard J, Broeckx G, Page DB, et al. Pitfalls in machine learning-based assessment of tumor-infiltrating lymphocytes in breast cancer: a report of the International Immuno-Oncology Biomarker Working Group on Breast Cancer. *J Pathol*. 2023;260(5):498–513. https://doi.org/10.1002/PATH.6155
35. Denkert C, Loibl S, Noske A, et al. Tumor-associated lymphocytes as an independent predictor of response to neoadjuvant chemotherapy in breast cancer. *J Clin Oncol*. 2010;28(1):105–113. https://doi.org/10.1200/JCO.2009.23.7370
36. Jiao Y, Li J, Qian C, Fei S. Deep learning-based tumor microenvironment analysis in colon adenocarcinoma histopathological whole-slide images. *Comput Methods Programs Biomed*. 2021;204:106047. https://doi.org/10.1016/J.CMPB.2021.106047
37. Graham S, Vu QD, Jahanifar M, et al. One model is all you need: multi-task learning enables simultaneous histology image segmentation and classification. *Med Image Anal*. 2023;83:102685. https://doi.org/10.1016/J.MEDIA.2022.102685
38. Wang X, Du Y, Yang S, et al. RetCCL: clustering-guided contrastive learning for whole-slide image retrieval. *Med Image Anal*. 2023;83:102645. https://doi.org/10.1016/J.MEDIA.2022.102645
39. Wölflein G, Ferber D, Meneghetti AR, et al. A good feature extractor is all you need for weakly supervised pathology slide classification. In: *European Conference on Computer Vision (ECCV) BioImage Computing Workshop. arXiv: 231111772*. Published online November 20, 2023. 2024. Accessed April 26, 2024. https://arxiv.org/abs/2311.11772v4
40. L'Imperio V, Wulczyn E, Plass M, et al. Pathologist validation of a machine learning-derived feature for colon cancer risk stratification. *JAMA Netw Open*. 2023;6(3):e2254891. https://doi.org/10.1001/JAMANETWORKOPEN.2022.54891
41. Reitsam NG, Grosser B, Enke JS, et al. Stroma AReactive invasion front areas (SARIFA): a novel histopathologic biomarker in colorectal cancer patients and its association with the luminal tumour proportion. *Transl Oncol*. 2024;44:101913. https://doi.org/10.1016/J.TRANON.2024.101913